Nonlocal, kinetic stimulated Raman scattering in nonuniform plasmas: Averaged variational approach

P. Khain,[1] L. Friedland,[1] A. G. Shagalov,[2] and J. S. Wurtele[3]
[1]*Racah Institute of Physics, Hebrew University of Jerusalem, Jerusalem 91904, Israel*
[2]*Institute of Metal Physics, Ekaterinburg 620219, Russian Federation*
[3]*Department of Physics, University of California, Berkeley, California 94720, USA*

(Received 7 June 2012; accepted 20 June 2012; published online 30 July 2012)

Excitation of continuously phase-locked (autoresonant) plasma waves in a nonuniform plasma via stimulated Raman backscattering is analyzed with a focus on the kinetic regime ($k\lambda_D \sim 1$). The dominant nonlinear effect in this regime is that of resonant particles, and the plasma wave excitation is a nonlocal process involving formation and transport of the electron phase space holes. Whitham's averaged variational principle is applied in studying the coupled plasma, laser pump, and seed waves dynamics. A flat-top electron velocity distribution is used as the simplest model allowing a variational formulation within the water bag theory. The corresponding Lagrangian, averaged over the fast phase variable, yields evolution equations for the slow field variables. The adiabatic multiple water bag extension of the theory for application to autoresonant plasma waves in nonuniform plasmas with more realistic initial distributions is also discussed. Numerical solutions of the system of slow variational equations are compared with Vlasov-Ampere simulations. © *2012 American Institute of Physics*. [http://dx.doi.org/10.1063/1.4737609]

I. INTRODUCTION

Stimulated Raman backscattering (RBS) in plasmas is a resonant three-wave interaction in which the energy flux of an incident laser wave (pump) is transferred to a plasma wave and a scattered electromagnetic wave (seed) is amplified in the backward direction.[1] This process is of great importance for inertial confinement fusion experiments (see Refs. 2–8, for example). In particular, RBS can potentially degrade the efficiency of laser absorption in the target by reflecting a fraction of the incident energy flux; furthermore, energetic electrons can be created which then preheat the target.[1] Alternatively, RBS can be turned into a beneficial mechanism and used for intense pulse compression in plasma-based Raman amplifiers.[9–12]

Since RBS is a resonant interaction, understanding frequency shifts in plasma waves is critical to developing a theory for saturation of the interaction. For low temperature ($k\lambda_d \lesssim 0.15$, k being the wave number, and λ_D the Debye length), fluid nonlinearity[13–18] produces a frequency shift in the plasma wave, while particle trapping becomes the dominant nonlinearity[19–22] for $k\lambda_d \gtrsim 0.25$. The theory in these papers assumes a homogenous plasma; this assumption, while analytically simplifying the analysis, ignores the coupling of the lasers into the plasma, plasma density gradients, and density gradients created by ion waves. The ion waves themselves can be created by stimulated Brillouin scattering (SBS). In the National Ignition Facility (NIF), stimulated Raman scattering (SRS) depletes specific pulses[23,24] through reflection and SBS (along with frequency detuning) is used to compensate[24,25] by transferring power from undepleted to depleted pulses. The geometric size and complexity, along with the large range of temporal and spatial scales, precludes a fully kinetic simulation of the laser-plasma interaction. Three-wave like codes are employed for modeling; incorporating nonlinear and kinetic effects in three-wave or fluid codes, derived from consideration of homogenous plasma, has been attempted with varying degrees of success.[26–30] These theoretical analyses assume a homogeneous plasma, thereby eliminating potentially significant nonlocal effects.

Plasma inhomogeneity was considered as a saturation mechanism for SRS (Ref. 31) and as a saturation (and to enhance selection of backscatter over forward scatter) for Raman compression.[11] It was recently noted[32] that, under specific conditions, the nonlinear RBS frequency shift due to fluid nonlinearities can be continuously compensated for by the linear frequency detuning (from three-wave resonance) caused by the density variation in the plasma. This regime is usually referred to as autoresonance. In general, autoresonance is a phenomenon of nonlinear physics, where a perturbed nonlinear system is captured into resonance and stays phase-locked with perturbing oscillations (or waves) despite variation of the system's parameters. For nearly half a century, studies of autoresonance were limited to relativistic gyroresonant wave-particle interactions (starting from Refs. 33 and 34 for particle accelerators), but many new applications of the autoresonance idea and progress in the theory emerged in the last two decades (for a review of some applications, see Refs. 35 and 36). A general theory of autoresonant three-wave interactions was reported in Ref. 37.

In the present work, we develop a self-consistent kinetic nonlocal theory of autoresonant RBS in a nonuniform plasma. This extends earlier work by Yaakobi *et al.*[32] by exploring the kinetic regime, where particle trapping dominates the dynamics. We use the Whitham's averaged variational principle,[38] valid if the length scales of variation of the plasma electric field amplitude and wave vector are large compared to the wavelength of the driving ponderomotive

potential. The averaged variational principle was developed by Whitham in the theory of slow modulations of nonlinear waves and comprises a nonlinear generalization of the Wentzel-Kramers-Brillouin (WKB) theory for linear waves. According to Whitham's approach, one averages the governing Lagrangian in a nonlinear wave propagation problem over the fast phase variable. Only slow dependent field variables remain in the averaged Lagrangian, which, upon variation with respect of these variables, yields slow evolution equations in the problem. The idea of using Whitham's principle in autoresonant nonlinear wave interactions was proposed in Refs. 39 and 40 and illustrated in the problem of excitation of large amplitude waves of the Sine-Gordon and Korteweg-de-Vries equations. Recently, this principle was used to describe the autoresonant evolution of Bernstein, Greene, and Kruskal (BGK) modes in uniform plasmas, using a chirped frequency driving field, and assuming a flat-top electron velocity distribution function.[41] In this paper, we focus on the stationary case, wherein the frequencies of the interacting waves remain constant, while the plasma density gradient and the associated spatial variation of wave vectors play the role of the frequency chirp.

This paper is organized as follows. In Sec. II, we briefly summarize earlier work on autoresonant RBS in an inhomogeneous plasma and discuss qualitative differences between the fluid and kinetic regimes. In Sec. III, we develop our simplified, flat-top (water bag) electron distribution model for the autoresonant RBS in a nonuniform plasma, formulate a Lagrangian theory based on this model, calculate the averaged Lagrangian, and derive slow variational equations describing the coupled evolution of the plasma wave, and the pump and seed electromagnetic waves. The theory is then compared with Vlasov simulations. In Sec. IV, we derive a multiple water bag approach to generalize from a water bag distribution to a Maxwellian velocity distribution and compare our results with Vlasov simulations. Finally, Sec. V contains our conclusions.

II. EARLIER RESULTS ON AUTORESONANT RBS IN INHOMOGENOUS PLASMAS

Recently, Yaakobi *et al.*[32] investigated autoresonance in RBS, focusing on the regime $k\lambda_D \ll 1$, where resonant particle (kinetic) effects can be neglected and the dominant nonlinear frequency shift of the plasma wave comes from a fluid-type nonlinearity. Their analysis reduced the nonlinear evolution of the plasma wave in a stationary, one-dimensional, underdense plasma with stationary ions to

$$\frac{\partial G}{\partial x} + i(\gamma|G|^2 + \alpha x)G = \frac{1}{6}AB^*, \tag{1}$$

where a positive density gradient ∇n in the direction of propagation is assumed and $A(x)$, $B(x)$, and $G(x)$ are the complex dimensionless envelopes of the pump, seed, and plasma wave electric fields ($E_{1,2}$ and E_x, respectively), such that $|A,B| = \frac{e|E_{1,2}|}{\sqrt{2}mu_{th}\omega_{1,2}}$ and $|G| = \frac{e\lambda_D|E_x|}{mu_{th}^2} \equiv E_g$. Here, $\omega_{1,2}$ (and ω in the following) are the frequencies of the laser (and plasma) waves, x is the dimensionless coordinate (rescaled by λ_D) along the density gradient, and u_{th} is the electron thermal velocity. The parameter $\gamma = \frac{\beta\omega\lambda_D}{6kc^2}$, where $\beta = \frac{15u_{th}^2c^2k^4}{\omega\omega_p^2}$, describes the nonlinearity in the problem and $\alpha = (6kL)^{-1}$, where $L = [\nabla n/n]^{-1}$is the spatial variation scale length. Equation (1) is the same as in Ref. 32, but with different notations adjusted to those used in our water bag theory in the following sections. The point $x = 0$ corresponds to the location of the exact three-wave resonance and the term in brackets in Eq. (1) describes the competing effects of the linear and nonlinear frequency shifts of the plasma wave. In autoresonance, one seeks a slow, phase locked ($\Phi = \arg A - \arg B - \arg G \approx \pm\pi/2$) solution for G and, consequently, neglects the term $\partial G/\partial x$ in Eq. (1). This yields a cubic equation $(\gamma|G|^2 + \alpha x)|G| = \pm\mu$ for $|G(\xi)|$, where $\mu = |AB^*|/6$. We solved the cubic equation for $|G|$ in Fig. 1 for parameters corresponding to a 1 keV plasma, laser intensities of $J_1 = 10^{17}\mathrm{W/cm^2}, J_2 = 10^{15}\mathrm{W/cm^2}$ for the pump and seed waves, respectively, and a vacuum pump wavelength of 351 nm. We neglected the depletion of these waves in Fig. 1. We used $k\lambda_D = 0.12$, which corresponds to a central density of $n_0 = 1.8 \times 10^{21}\mathrm{cm^{-3}}$ and assumed $L = 13.5\,\mu\mathrm{m}$. The different branches for the solution to the cubic are evident in Fig. 1.

One observes a region with negative x, where three solutions are allowed, while for positive x (i.e., beyond linear resonance), only one solution is possible. This behavior is characteristic of nonlinear resonance.[42] The two stable branches $E_g^{\pm}$ correspond to the phase mismatch Φ being locked at $\pm\frac{\pi}{2}$, respectively. These solutions proceed from zero at $x = \mp\infty$ for a plasma wave propagating either in the direction of increasing or decreasing plasma density. One observes that if the plasma wave propagates from large negative x, i.e., in the direction of the plasma density gradient,[43] it reaches a "knee." At the knee, the derivative $\partial G/\partial x \to \infty$ and should not be neglected. The slow autoresonant growth of the plasma wave discontinues as the plasma wave dephases from resonance and the wave breaks prior to reaching linear resonance. Importantly, this result is characteristic of the regime $k\lambda_D \ll 1$, where the nonlinear shift scales quadratically with the plasma amplitude.[13–15,17,18,45] In the

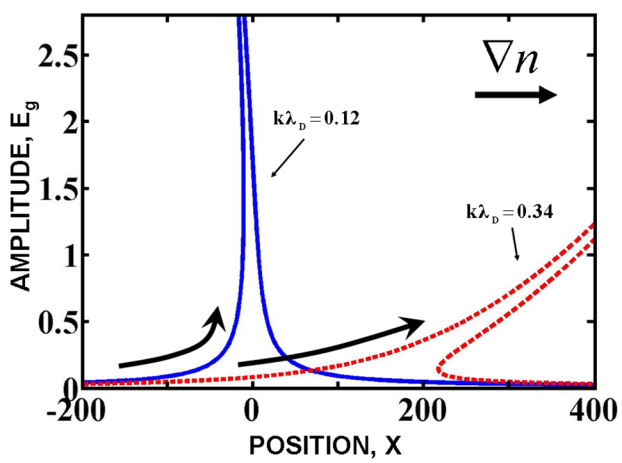

FIG. 1. Autoresonant solutions for the plasma wave amplitude in the warm fluid model of Ref. 32 for $k\lambda_D = 0.12$ (blue solid lines) and $k\lambda_D = 0.34$ (red dashed lines) regimes.

regime where $k\lambda_D \sim O(1)$ (typically $k\lambda_D > 0.25$), the dominant nonlinearity of the plasma arises from effects associated with trapped particles.[19–22]

For an uniform plasma saturation from particle trapping was first studied, for small nonlinearity, by Morales and O'Neil.[44] They demonstrated that the nonlinear frequency shift should scale with the square root of the wave amplitude and has an opposite sign as compared to that of the fluid nonlinearity. In addition, Dewar[45] drew attention to the nonuniqueness of the allowed distributions of trapped particles in the problem and examined how it affects the nonlinear shifts in important limits of adiabatic and sudden turn-on of the wave in an uniform plasma. The detailed nonlinear dependence of the frequency shift on the amplitude of the plasma wave also depends on the plasma temperature ($k\lambda_D$) and the square root dependence reflects but a limited range of the possible frequency shifts.[22] Based on the results of Ref. 44, Chapman *et al.*[46,47] substituted $\gamma|G|^2 \rightarrow -\gamma'|G|^{1/2}$ in Eq. (1), where $\gamma' = \frac{\eta\omega^2\sqrt{\lambda_D}}{3u_{th}\omega_p\sqrt{k}}$ and $\eta = 0.4$. They proceeded to study autoresonant plasma evolution of RBS in a nonuniform plasma in the kinetic regime using this modified three-wave interaction model. A similar model was also used by Williams *et al.*[48] in describing kinetic autoresonance in SBS. An example of autoresonant excitation with a nonlinear frequency shift corresponding to that used in Ref. 46 and with $k\lambda_D = 0.34$ (so that it is in the regime where particle trapping is significant) is also plotted in Fig. 1. The same plasma, pump, and seed parameters were used as for the $k\lambda_D = 0.12$ case, but the central plasma density was now $n_0 = 4.5 \times 10^{20}\text{cm}^{-3}$. The switch to a different type of nonlinearity in the frequency shift did not affect the linear excitation stage of the plasma wave, but the change in sign of the nonlinearity removed the breaking "knee" on the wave branch propagating in the direction of the density gradient (the direction of the arrow on the autoresonant branch corresponding to Ref. 46 model in Fig. 1). This allowed continuation of the phase-locked solution and autoresonant excitation of the plasma wave beyond the linear resonance.

The aforementioned switch between different nonlinear frequency shift models in the RBS process at some $k\lambda_D$ poses a number of unresolved issues when applied to nonuniform plasmas. For instance, how should one apply the theory as $k\lambda_D$ varies along the density gradient and crosses the (imprecisely defined) boundary of applicability between the two models? Moreover, there remains the critical issue of nonlocality. Morales and O'Neil's theory[44] was developed for an uniform plasma. Their particles were trapped in the wave troughs and produced, in the nonlinear stage, plateau regions in phase space distribution function, similar to those seen in the nonlinear stage of Landau damping. In contrast, in a nonuniform plasma, resonantly trapped particles may move with the wave from low to high density regions, thereby forming holes (depletions) in phase space instead of plateaus. The effect is due to the nonlocal "memory" of distribution functions described by the Vlasov equation (which governs the electron kinetics) and, in some cases, this non-locality of the resonant interaction should be taken into account. For example, Friedland *et al.*[41,49,50] described the formation of phase space holes in a Vlasov plasma driven by a chirped frequency perturbation, such that the driving phase velocity decreases and passes from the velocity tail of the electron distribution function to the bulk. These holes were phase-locked to the driving wave and yielded stable autoresonant BGK modes[51] via the coupling to the Poisson equation. Formation of pairs of phase space holes and clumps was also studied by Berk *et al.*[52–54]

III. KINETIC RBS IN A NONUNIFORM WATER BAG PLASMA MODEL

A. The model

Our simplified one-dimensional (1D), kinetic RBS theory uses a flat-top nonuniform density water bag model.

The uniform phase space distribution of plasma electrons is confined between two limiting trajectories $u_{1,2}(x,t)$ and vanishes outside the trajectories as illustrated in Fig. 2. We assume a stationary ion background of nonuniform density $\rho(x)$, describe the plasma wave via the potential $U(x,t)$, and represent the electromagnetic waves by their total vector potential $A(x,t)$. The system is governed by the momentum, Poisson, and wave equations

$$u_{1,2t} + u_{1,2}u_{1,2x} = (U - A^2)_x, \tag{2}$$

$$U_{xx} = \frac{1}{2\sqrt{3}}(u_1 - u_2) - \rho(x), \tag{3}$$

$$A_{tt} - \nu^2 A_{xx} + \frac{1}{2\sqrt{3}}(u_1 - u_2)A = 0. \tag{4}$$

All dependent and independent variables in this system are dimensionless. We scaled the ion density by its value $n_0 = n(x=0)$ and normalized limiting electron velocities by $u_0 = u_{th}/\sqrt{3}$, where u_{th} is the unperturbed absolute value of the (assumed equal) dimensional velocities $u_{1,2}(x=0)$; time and space variables, t and x, are scaled by the unperturbed

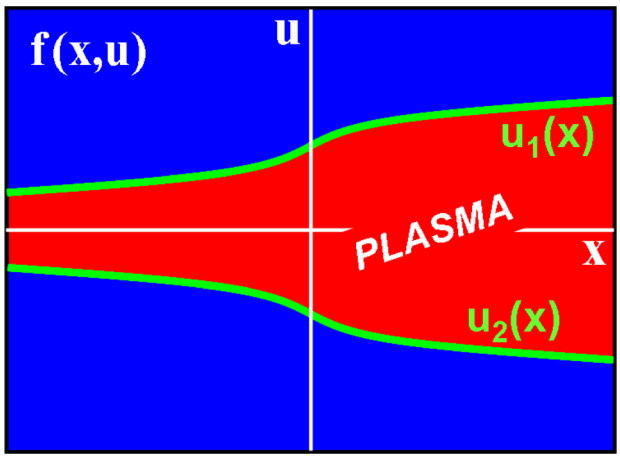

FIG. 2. Flat-top electron phase-space distribution in an one-dimensional nonuniform plasma. The distribution has values of either $f=0$ (blue) or $f = constant$ (red).

inverse plasma frequency $\omega_p^{-1} = (4\pi e^2 n_0/m)^{-1/2}$ and $\lambda_D = u_0/\omega_p$, respectively and $\nu = c/u_0$. Finally, the potentials U and A are normalized by mu_0^2/e and mcu_0/e, respectively. The factor $\sqrt{3}$ in u_0 introduced in these normalizations ensures that if one neglects the electromagnetic waves and linearizes the system around the equilibrium $u_{1,2}^0 \approx \pm u(x) = \sqrt{3}\rho(x)$, $U^0 \approx 0$, one obtains the expected local dispersion relation for the plasma wave

$$\omega^2 = \rho + 3k^2\rho^2. \tag{5}$$

In other words, for an uniform plasma, with $\rho = 1$, we obtain the same dispersion relation $\omega^2 = 1 + 3k^2$ as in the warm fluid approximation. The similarity of our nonuniform water bag model with the warm fluid approximation extends beyond the linear case.[14] Indeed if, for zero A, we define $N = (u_1 - u_2)/(2\sqrt{3})$ and $V = (u_1 + u_2)/2$, Eqs. (2) and (3) can be rewritten as

$$V_t + VV_x = U_x - 3NN_x, U_{xx} = N - \rho(x), \tag{6}$$

which is the standard nonlinear electron fluid model with fixed ions and pressure $P = N^3$. The similarity is complete, as long as the structure of the phase space is similar to that in Fig. 2. However, we will see below that in the case of RBS in a nonuniform plasma, the phase space occupied by the electrons can become more complex, as phase space holes (bubbles) are formed inside the distribution function when a driven plasma wave propagates in the direction of the density gradient. Prior to pursuing our theoretical approach to RBS in nonuniform water bag plasmas, we present Vlasov simulation results.

B. Vlasov simulations

Our simulations solve the general Vlasov-Ampere system for the electron phase space distribution, $f(x,u,t)$, and the electrostatic self-field, $E(x,t)$. Thus, they can go beyond the flat-top distribution model described above; they will be used later as well when we study initially Maxwellian distributions. However, for simplicity, we assume a prescribed, constant amplitude ponderomotive driving field $E_d = \varepsilon \sin(k_d x - \omega_d t)$ acting on electrons, where the driving frequency is given by the pump/seed frequency mismatch $\omega_d = \omega_1 - \omega_2$ and remains constant, while $k_d = k_1 + k_2 \approx const$ because of the assumed subcriticality of the plasma density ($\omega_{1,2} \gg \omega_p$). Thus, we solve a 1D, *driven* Vlasov-Ampere system for $f(x,u,t)$ and $E(x,t)$

$$f_t + uf_x - (E + E_d)f_u = 0, \quad E_t = \int ufdu. \tag{7}$$

Here, again, all dependent and independent variables and parameters are dimensionless (E and E_d are scaled, as above, by $mu_0\omega_p/e$). We assume an initially neutral plasma, where the electron density balances a linearly increasing density $\rho = 1 + x/L$ of stationary ions (both x and L are scaled with respect to λ_D). We solved our system numerically, using a centered finite difference scheme in x, Fourier transform in u, and a leap-frog integration scheme in time. The accuracy of our code was tested by varying the number of spectral harmonics in u, as well as by optimizing the values of t and x - steps.

Examples of simulation results are presented in Figs. 3 and 4 for $k_d = 0.12$ and $k_d = 3$, respectively. We solved the system in the phase-space region $-L/2 < x < L/2$, $-u_m < u < u_m$ (we used $u_m = 8$) for the flat-top initial velocity distribution,

$$f_0 \equiv f(u,x,0) = \begin{cases} \rho/(2\sqrt{3}) & |u| < \sqrt{3}\rho \\ 0 & |u| > \sqrt{3}\rho \end{cases}$$

(the realistic Maxwell distribution will be discussed in Sec. IV). To avoid singularities characteristic of the Vlasov equation with sharp boundaries in phase space we smoothed the distribution boundaries in velocity space, using $f_0 = (1/4\sqrt{3})\{\tanh[(u + \sqrt{3}\rho)/u_s] - \tanh[(u - \sqrt{3}\rho)/u_s]\}$, where $u_s = 0.17$. We introduced artificial high frequency filters at grid scales in x and u. Using the plasma parameters from Sec. II for the case of $k_d = 0.12$, we obtained the driving field amplitude $\varepsilon = 0.0028$ and its phase velocity $u_d = \omega_d/k_d = 8.34$. The blue solid line in Fig. 3(a) shows the waveform of the oscillating component of the electric field (the slow averaged component was subtracted) of the excited plasma wave at the final time of the simulation ($t_f = 300$), while the dashed red line shows the envelope of the electric field obtained from our variational theory (see Sec. III C). The associated phase space electron distribution function is presented in Fig. 3(b) (blue for $f(x,u) = 0$ and red for $f(x,u) = (2\sqrt{3})^{-1}$). The wave grows with x until it nearly reaches $x = 0$; at that point it breaks due to detuning from the driving field. This wave breaking is typical for the warm fluid-type regime (dimensionless $k \ll 1$), as discussed in Sec. II.

On the other hand, in the kinetic regime ($k \sim O(1)$), the spatial evolution is qualitatively different. This is illustrated in Fig. 4, where we consider $k_d = 3$, $\varepsilon = 0.069$, and

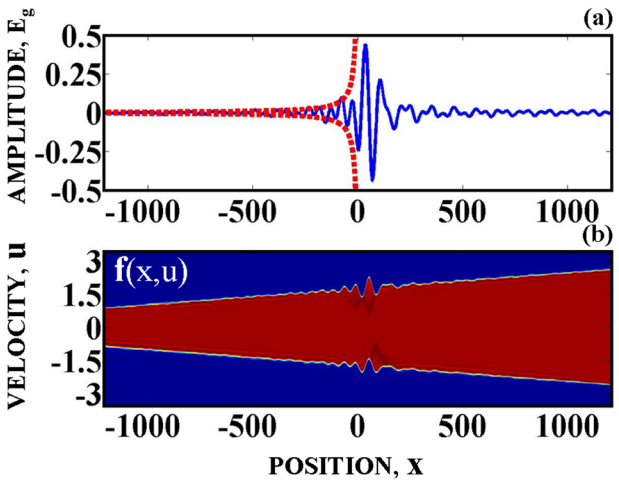

FIG. 3. Plasma wave formation in the warm fluid $k\lambda_D = 0.12$ regime for an initially flat-top electron phase space distribution. (a) The plasma wave amplitude from the variational theory (red dashed line) and numerical simulations (blue solid line). (b) The associated electron distribution function. Note that no autoresonance occurs in this case.

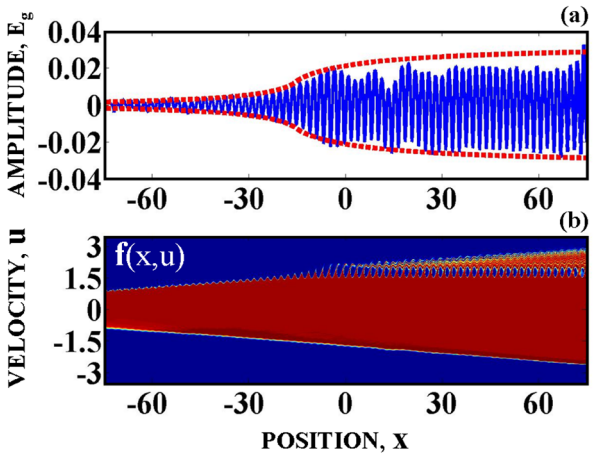

FIG. 4. Plasma wave formation in the kinetic $k\lambda_D = 3$ regime for initially flat-top electron phase space distribution. (a) The plasma wave amplitude from the variational theory (red dashed line) and numerical simulations (blue solid line). (b) The associated electron distribution function.

$u_d = 1.764$ (the same plasma and driving parameters as in the previous case, but with a central density of $n_0 = 2.4 \times 10^{18}\text{cm}^{-3}$), and the final time $t_f = 100$. The plasma wave (solid blue line) continues beyond $x = 0$ (Fig. 4(a)) and a chain of phase-space holes in the electron distribution appears beyond this point (Fig. 4(b)). Qualitatively, the formation of the phase space holes can be explained as follows. Initially, empty phase-space regions are trapped in the driving wave troughs (at $x < 0$ and $u \simeq u_d$) and are carried by the wave into the bulk of the distribution (at $x > 0$ and $u \simeq u_d$). These holes are phase-locked with the driving wave and are associated with a stable autoresonant BGK mode.[49] Formation of the holes requires modification of the water bag model described above, because in addition to two limiting trajectories prior to formation of the holes, there appear *new* phase space boundaries associated with the holes beyond some point in x. Consequently, we model this part of the problem by the system (compare to Eqs. (2)–(4))

$$u_{1,2t} + u_{1,2}u_{1,2x} = (U - A^2)_x, \tag{8}$$

$$u_{\pm t} + u_{\pm}u_{\pm x} = (U - A^2)_x, \tag{9}$$

$$U_{xx} = \frac{1}{2\sqrt{3}}[u_1 - u_2 - (u_+ - u_-)] - \rho, \tag{10}$$

$$A_{tt} - \nu^2 A_{xx} + \frac{1}{2\sqrt{3}}[u_1 - u_2 - (u_+ - u_-)]A = 0, \tag{11}$$

where the effect of phase space holes is described by $u_{\pm}(x,t)$ representing the upper and lower parts of the holes boundaries. The averaged variational theory based on switching between these two models is presented in Sec. III C.

C. Lagrangian RBS theory for a flat-top electron distribution

We begin with the case without phase space holes. With auxiliary potentials $\psi_{1,2}$, such that $u_{1,2} = (\psi_{1,2})_x$, our system (2)–(4) can be derived from the variational principle $\delta \int L dx dt = 0$, where the 4-field ($\psi_{1,2}$, U, and A) Lagrangian is

$$\begin{aligned} L_1 = &\left[\frac{1}{2\sqrt{3}}(\psi_{1x} - \psi_{2x}) - \rho\right](U - A^2) \\ &- \frac{1}{4\sqrt{3}}(\psi_{1x}\psi_{1t} - \psi_{2x}\psi_{2t}) - \frac{1}{12\sqrt{3}}(\psi_{1x}^3 - \psi_{2x}^3) \\ &+ \frac{1}{2}U_x^2 + A_t^2 - \nu^2 A_x^2 - \rho A^2. \end{aligned} \tag{12}$$

Similarly, for positions x that include phase space holes, we switch to Eqs. (8)–(11), introduce additional auxiliary potentials $\psi_{\pm}$ via $v_{\pm} = \psi_{\pm x}$, and write the 6-field ($\psi_{1,2}$, $\psi_{\pm}$, U, and A) Lagrangian which includes phase space holes

$$\begin{aligned} L_2 = &\left[\frac{1}{2\sqrt{3}}(\psi_{1x} - \psi_{2x} - \psi_{+x} + \psi_{-x}) - \rho\right](U - A^2) \\ &- \frac{1}{4\sqrt{3}}(\psi_{1x}\psi_{1t} - \psi_{2x}\psi_{2t} - \psi_{+x}\psi_{+t} + \psi_{-x}\psi_{-t}) \\ &- \frac{1}{12\sqrt{3}}(\psi_{1x}^3 - \psi_{2x}^3 - \psi_{+x}^3 + \psi_{-x}^3) \\ &+ \frac{1}{2}U_x^2 + A_t^2 - \nu^2 A_x^2 - \rho A^2. \end{aligned} \tag{13}$$

Next, we consider a stationary RBS process and, in view of the slow spatial variation of the ion density, apply Whitham's averaged variational principle.[38] We write the plasma and electromagnetic wave potentials as $U = b(x) + a(x)\cos\theta$ and $A_{1,2} = a_{1,2}(x)\cos\theta_{1,2}$, where the wave amplitudes b, a, and $a_{1,2}$ are assumed to be slow functions of x. The phases θ and $\theta_{1,2}$ are fast variables, the frequencies $\omega = -\partial\theta/\partial t$ and $\omega_{1,2} = -\partial\theta_{1,2}/\partial t$ remain constant, and the wave vectors $k(x) = \partial\theta/\partial x$ and $k_{1,2}(x) = \partial\theta_{1,2}/\partial x$ are slow functions of x. Furthermore, in seeking phase-locked (autoresonant) three-wave solutions, we assume that the frequencies of the waves are matched, $\omega = \omega_1 - \omega_2$, and that the phase mismatch $\Phi = \theta_1 - \theta_2 - \theta$ is a slow function of x. For the auxiliary potentials describing the limiting trajectories, we seek solutions of form $\psi_{1,2} = \xi_{1,2}(x) + \Psi_{1,2}(\theta)$, and similarly $\psi_{\pm} = \xi_{\pm}(x) + \Psi_{\pm}(\theta)$, where $\Psi_{1,2}(\theta)$ and $\Psi_{\pm}(\theta)$ are 2π-periodic in θ, while $\beta_{1,2}(x) = \partial\xi_{1,2}/\partial x$ and $\beta_{\pm}(x) = \partial\xi_{\pm}/\partial x$ (the averaged velocities of the limiting trajectories) are slow functions of x. Note that we are using a single harmonic approximation for the plasma and laser waves, and a full nonlinear representation for the limiting trajectories. This assumption requires sufficiently small amplitude waves, but does not exclude fully nonlinear development of the limiting trajectories during the formation of the phase space holes (see a similar approach in Refs. 41 and 50 and in a recent paper by Dodin and Fisch[55]).

The next step in the theory is to perform Witham's averaging of the Lagrangians over the fast phases $\theta, \theta_{1,2}$. The details of the averaging procedure are given in Appendix A; here, we present the final results. The averaged Lagrangian without phase space holes is

$$\overline{L}_1 = b\left(\frac{\beta_1-\beta_2}{2\sqrt{3}}-\rho\right)+\frac{k^2}{4}a^2-\frac{\beta_1-\beta_2}{4\sqrt{3}}(a_1^2+a_2^2) - \frac{1}{6\sqrt{3}}(\langle s_1^3\rangle-\langle s_2^3\rangle)+\frac{1}{2\sqrt{3}}\left(\frac{\omega}{k}-\beta_1\right)B_1 - \frac{1}{2\sqrt{3}}\left(\frac{\omega}{k}-\beta_2\right)B_2+\frac{1}{4\sqrt{3}}\frac{\omega}{k}(\beta_1-\beta_2)\left(\frac{\omega}{k}-\beta_1-\beta_2\right) + \frac{a_1^2}{2}(\omega_1^2-\nu^2k_1^2)+\frac{a_2^2}{2}(\omega_2^2-\nu^2k_2^2) \quad (14)$$

and with phase space holes is

$$\overline{L}_2 = b\left(\frac{\beta_1-\beta_2-\beta_++\beta_-}{2\sqrt{3}}-\rho\right)+\frac{k^2}{4}a^2 - \frac{\beta_1-\beta_2-\beta_++\beta_-}{4\sqrt{3}}(a_1^2+a_2^2) - \frac{1}{6\sqrt{3}}(-\langle s_1^3\rangle-\langle s_2^3\rangle+\langle s_+^3\rangle+\langle s_-^3\rangle) + \frac{1}{2\sqrt{3}}\left(\frac{\omega}{k}-\beta_1\right)B_1-\frac{1}{2\sqrt{3}}\left(\frac{\omega}{k}-\beta_2\right)B_2 - \frac{1}{2\sqrt{3}}\left(\frac{\omega}{k}-\beta_+\right)B_++\frac{1}{2\sqrt{3}}\left(\frac{\omega}{k}-\beta_-\right)B_- + \frac{1}{4\sqrt{3}}\frac{\omega}{k}\begin{bmatrix}(\beta_1-\beta_2)\left(\frac{\omega}{k}-\beta_1-\beta_2\right)\\ -(\beta_+-\beta_-)\left(\frac{\omega}{k}-\beta_+-\beta_-\right)\end{bmatrix} + \frac{a_1^2}{2}(\omega_1^2-\nu^2k_1^2)+\frac{a_2^2}{2}(\omega_2^2-\nu^2k_2^2), \quad (15)$$

where $B_{1,2}(x), B_\pm(x)$ are the slow electron energies associated with $u_{1,2}, u_\pm$ trajectories, respectively (see Appendix A for the definitions). Here,

$$\langle s_{1,2}^3\rangle = \frac{1}{2\pi}\int_0^{2\pi}\{2[B_{1,2}+(a-a_1a_2\cos\Phi)\cos\theta]\}^{3/2}d\theta$$

and

$$\langle s_\pm^3\rangle = \frac{1}{2\pi}\int_0^{\theta_\pm}\{2[B_\pm+(a-a_1a_2\cos\Phi)\cos\theta]\}^{3/2}d\theta,$$

where

$$\theta_\pm = \arccos\left[-\frac{B_\pm}{a-a_1a_2\cos\Phi}\right].$$

Our averaged Lagrangians are functions of slow variables only: $\overline{L}_1=\overline{L}_1(b,a,a_{1,2},B_{1,2},\beta_{1,2},k,k_{1,2},\Phi)$ and $\overline{L}_2=\overline{L}_2(b,a,a_{1,2},B_{1,2},B_\pm,\beta_{1,2},\beta_\pm,k,k_{1,2},\Phi)$. We obtain the desired system of slow equations by taking variations of $\overline{L}_{1,2}$ with respect to these slow variables. For example, in the case without phase-space holes, variation with respect to b yields the quasi-neutrality condition

$$\beta_1-\beta_2=2\sqrt{3}\rho. \quad (16)$$

The variation with respect to a yields the dispersion relation for the plasma wave

$$\sqrt{3}k^2a=\langle(s_1-s_2)\cos\theta\rangle. \quad (17)$$

The variations with respect to $B_{1,2}$ lead to

$$\langle s_{1,2}\rangle=\frac{\omega}{k}-\beta_{1,2}, \quad (18)$$

while the variations with respect to $a_{1,2}$ results in dispersion relations for the pump and seed waves, respectively

$$a_{1,2}(\rho-\omega_{1,2}^2+\nu^2k_{1,2}^2)=\frac{k^2}{2}a_{2,1}a\cos\Phi. \quad (19)$$

The variation with respect to $\xi_{1,2}$ yields energy conservation relations

$$B_{1,2}-b+\frac{\omega}{k}\left(\beta_{1,2}-\frac{\omega}{2k}\right)+\frac{a_1^2+a_2^2}{2}=C_{1,2}, \quad (20)$$

where $C_{1,2}$ are constants. Finally, the variations with respect to θ,θ_1,θ_2 result in

$$\left\{ka^2-\frac{\omega}{k^2}\left[\frac{B_1-B_2}{\sqrt{3}}+\rho\left(\frac{2\omega}{k}-\beta_1-\beta_2\right)\right]\right\}_x=k^2a_1a_2a\sin\Phi \quad (21)$$

and

$$(k_1a_1^2)_x=-(k_2a_2^2)_x=\frac{k^2}{2\nu^2}a_1a_2a\sin\Phi. \quad (22)$$

These equations yield the Manley-Rowe relations between the amplitudes $a, a_{1,2}$ of the three resonantly interacting wave potentials (e.g., $k_1a_1^2+k_2a_2^2=const$). We close this system of equations by adding the definition of the phase mismatch Φ

$$\Phi_x=k_1-k_2-k. \quad (23)$$

Similarly, by taking variations of $\overline{L}_2$, we obtain the slow evolution system for the case with the phase-space holes

$$\beta_1-\beta_2-\Delta u=2\sqrt{3}\rho, \quad (24)$$

$$\sqrt{3}k^2a=\langle(s_++s_--s_1-s_2)\cos\theta\rangle, \quad (25)$$

$$\mp\langle s_{1,2}\rangle=\frac{\omega}{k}-\beta_{1,2}, \quad (26)$$

$$\frac{\Delta u}{2}=\langle s_0\rangle, \quad (27)$$

$$a_{1,2}(\rho-\omega_{1,2}^2+\nu^2k_{1,2}^2)=\frac{k^2}{2}a_{2,1}a\cos\Phi, \quad (28)$$

$$B_{1,2}-b+\frac{\omega}{k}\left(\beta_{1,2}-\frac{\omega}{2k}\right)+\frac{a_1^2+a_2^2}{2}=C_{1,2}, \quad (29)$$

$$\left\{ka^2-\frac{\omega}{k^2}\left[\frac{B_1-B_2}{\sqrt{3}}+\rho\left(\frac{2\omega}{k}-\beta_1-\beta_2-\Delta u\right)\right]\right\}_x = k^2a_1a_2a\sin\Phi, \quad (30)$$

$$(k_1 a_1^2)_x = -(k_2 a_2^2)_x = \frac{k^2}{2\nu^2} a_1 a_2 a \sin\Phi, \tag{31}$$

$$\Phi_x = k_1 - k_2 - k, \tag{32}$$

where we set $B_+ = B_- \equiv B_0$ and, consequently, $\langle s_+ \rangle = \langle s_- \rangle \equiv \langle s_0 \rangle$. We also defined $\Delta u \equiv \beta_+ - \beta_- = 2\left(\frac{\omega}{k^*} - \beta_1^*\right)$ (k^*, β_1^* being the values of k, β_1 at $x = x^*$ where the holes are formed, respectively). A similar set of equations was obtained via Whitham's variational principle in Ref. 41 for the case of an uniform plasma driven by a prescribed, chirped frequency external ponderomotive potential.

As a first test of our theory, we solved the slow equations for the spatial evolution of the plasma wave electric field amplitude $E_g = ka$ assuming a prescribed, fixed amplitude, ponderomotive drive for comparison with the results of our numerical simulations in Figs. 3 and 4. For simplicity, we also assumed ideal phase locking, i.e., $\Phi = \pi/2$, prescribed (constant) amplitudes $a_{1,2}$ and two values for $k_d = k_1 - k_2 = 0.12$ (dashed red line in Fig. 3(a)) and $k_d = 3$ (dashed red line in Fig. 4(a)). One observes good agreement with simulations, illustrating both the wave breaking (prior to the formation of a hole) in the warm fluid regime ($k_d = 0.12$), and continuing spatially autoresonant growth of the excited plasma in the kinetic regime ($k_d = 3$). In Sec. IV, we present simulations and theory for phase space distributions that are initially Maxwellian in velocity and spatially nonuniform. We will also discuss the action flux redistribution between the interacting waves during the RBS in the fluid and kinetic regimes.

IV. KINETIC RBS FOR A MAXWELLIAN DISTRIBUTION

A. Vlasov-Ampere simulations

We proceed by presenting two examples of Vlasov-Ampere simulations for an initially Maxwellian distribution $f_0(x,u) = [\rho(x)/\sqrt{2\pi}]\exp(-u^2/2)$ and a fixed amplitude ponderomotive drive, similar to that used in Sec. III. We also use the same normalized variables and parameters as before, but with $u_0 = u_{th}$. The warm fluid regime of $k_d = 0.12$ (with the same plasma and driving parameters as for the flat-top distribution in Sec. III, i.e., $\varepsilon = 0.0028$ and $u_d = 8.34$) is presented in Fig. 5.

The blue solid line in Fig. 5(a) shows the waveform of the oscillating component of the electric field of the excited plasma wave at the final time of the simulation ($t_f = 300$), and the dashed red line shows the envelope $E_g = ka$ of the electric field obtained from our variational theory (see Subsection IV B). The associated phase space distribution function is seen in Fig. 5(b). The wave grows significantly with x until nearly reaching $x = 0$; at that point, it breaks. This result is very similar to that in Fig. 3 for a flat-top distribution. The reason for this similarity is that the effect of the detailed shape of the distribution is negligible in the warm fluid regime, where $u_d \gg 1$. Note that only a very weak plasma wave signal is seen at large x beyond the linear resonance. As one increases k_d, our simulations show similar plasma wave breaking near the linear resonance ($x \approx 0$) until k_d passes unity and the corresponding spatial evolution of the

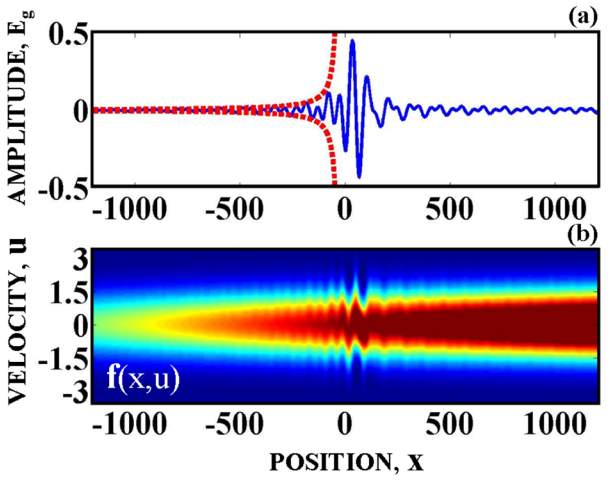

FIG. 5. Plasma wave excitation in the warm fluid $k\lambda_D = 0.12$ regime for an initially Maxwellian phase space distribution. (a) The plasma wave amplitude from the multiple water bag variational theory (red dashed line) and numerical simulations (blue solid line). (b) The associated distribution function.

driven plasma wave changes drastically. This effect is illustrated in Fig. 6, where we present an example for $k_d = 1$ and $\varepsilon = 0.023$, $u_d = 2$ (the same plasma and driving parameters as in Sec. III, but with a central density of $n_0 = 6 \times 10^{19}\text{cm}^{-3}$) and $t_f = 250$. Figure 6(a) shows that the plasma wave exhibits a continuous spatial growth via the formation of a chain of phase-locked phase space holes in the distribution (Fig. 6(b)). The effect is similar to that illustrated in Fig. 4 for the flat-top distribution. One may observe a very good agreement with the averaged variational theory (the dashed red envelope in Fig 6(a)). This theory for the Maxwellian case is described in Sec. IV B.

B. Averaged variational theory for a multiple water bag distribution

The following kinetic RBS theory uses a multiple water bag model. We model the initial distribution $f_0(x,u)$ as a

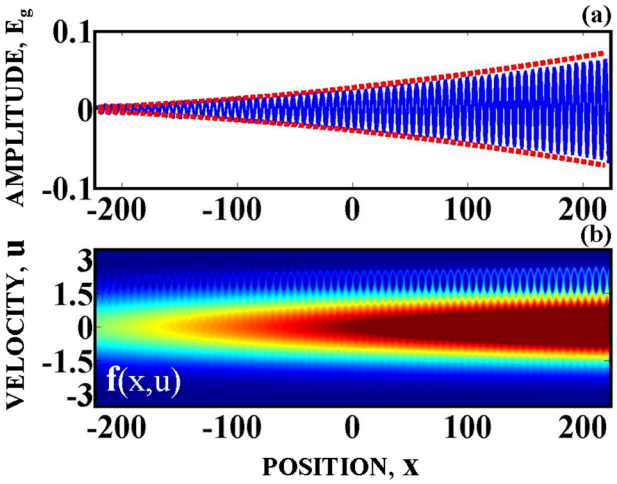

FIG. 6. Plasma wave excitation in the kinetic $k\lambda_D = 1$ regime for an initially Maxwellian phase space distribution. (a) The plasma wave amplitude from the variational theory (red dashed line) and numerical simulations (blue solid line). (b) The associated distribution function.

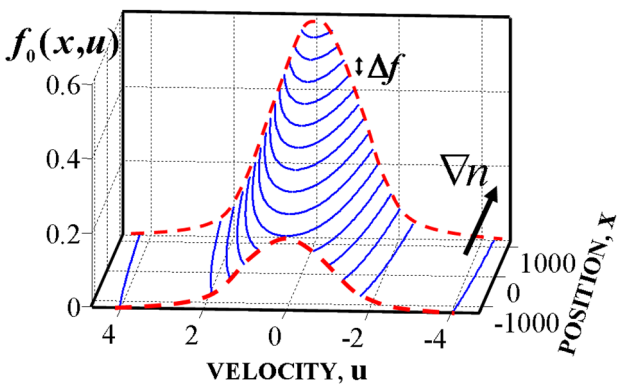

FIG. 7. Multi-water bag model for Maxwellian phase-space distribution in an one-dimensional nonuniform plasma.

superposition of M ($M=400$ in the examples below) flat-top layers of equal thickness, Δf (see Fig. 7).

In the case of a Maxwellian $f_0(x,u)=[\rho(x)/\sqrt{2\pi}]\exp(-u^2/2)$, the initial limiting trajectories of the mth layer are defined as

$$u^m_{1,2}(t=0,x)=\pm\sqrt{2\ln\left(\frac{\rho(x)}{\sqrt{2\pi}f^m_0}\right)}, \tag{33}$$

where $f^m_0=m\Delta f$ is the height of the mth layer. Later (at $t>0$), each layer is driven by the combination of the ponderomotive and self-fields and evolves similarly to the single layer described above. In other words, each layer is viewed as a flat-top distribution confined between two $u^m_{1,2}(x,t)$ or four $u^m_{\pm,1,2}(x,t)$ adiabatically varying limiting trajectories (depending on whether the hole is outside or inside the layer, respectively). We refer to the sets of indices m of layers which include or do not include a hole (at a given time t) as m'' and m', respectively. The problem is then governed by a set of M momentum equations (compare to Eqs. (8) and (9))

$$u^m_{1,2t}+u^m_{1,2}u^m_{1,2x}=(U-A^2)_x, \tag{34}$$

$$u^m_{\pm t}+u^m_{\pm}u^m_{\pm x}=(U-A^2)_x, \tag{35}$$

the Poisson equation (compare to Eq. (10))

$$U_{xx}=Q\Delta f-\rho(x), \tag{36}$$

where $Q=\sum_{m\in m'}(u^m_1-u^m_2)+\sum_{m\in m''}(u^m_1-u^m_2-u^m_++u^m_-)$, and the wave equation (compare to Eq. (11))

$$A_{tt}-\nu^2A_{xx}+Q\Delta fA=0. \tag{37}$$

Our system (34)–(37) can be derived from the variational principle $\delta\int L dxdt=0$, where the $(4M+2)$-field ($\psi^m_{1,2}$, $\psi^m_{\pm}$, U, and A) Lagrangian is

$$L=(\Delta fR_1-\rho)(U-A^2)-\frac{\Delta f}{2}R_2-\frac{\Delta f}{6}R_3+\frac{1}{2}U^2_x+(A^2_t-\nu^2A^2_x-\rho)A^2, \tag{38}$$

where $\psi^m_{1,2}$,$\psi^m_{\pm}$ are auxiliary potentials for the velocities of the limiting trajectories of the mth layer and

$$R_1=\sum_{m\in m'}(\psi^m_{1x}-\psi^m_{2x})+\sum_{m\in m''}(\psi^m_{1x}-\psi^m_{2x}-\psi^m_{+x}+\psi^m_{-x}), \tag{39}$$

$$R_2=\sum_{m\in m'}(\psi^m_{1x}\psi^m_{1t}-\psi^m_{2x}\psi^m_{2t})+\sum_{m\in m''}(\psi^m_{1x}\psi^m_{1t}-\psi^m_{2x}\psi^m_{2t}-\psi^m_{+x}\psi^m_{+t}+\psi^m_{-x}\psi^m_{-t}), \tag{40}$$

$$R_3=\sum_{m\in m'}[(\psi^m_{1x})^3-(\psi^m_{2x})^3]+\sum_{m\in m''}[(\psi^m_{1x})^3-(\psi^m_{2x})^3-(\psi^m_{+x})^3+(\psi^m_{-x})^3]. \tag{41}$$

As before, we consider a stationary RBS process and apply Whitham's averaged variational principle. We seek solutions of the form $\psi^m_{1,2}=\xi^m_{1,2}(x)+\Psi^m_{1,2}(\theta)$, and similarly $\psi^m_{\pm}=\xi^m_{\pm}(x)+\Psi^m_{\pm}(\theta)$, where $\Psi^m_{1,2}(\theta)$ and $\Psi^m_{\pm}(\theta)$ are 2π-periodic in θ, while $\beta^m_{1,2}(x)=\partial\xi^m_{1,2}/\partial x$ and $\beta^m_{\pm}(x)=\partial\xi^m_{\pm}/\partial x$ are slow functions of x. We again use a single harmonic approximation for the plasma and laser waves. Next, we average the Lagrangian (38) over the fast phases $\theta,\theta_{1,2}$. The details of the averaging procedure are similar to those of the single layer (flat-top) distribution described in Appendix A. Here, we present the final result for the averaged Lagrangian

$$\overline{L}=-\rho b+\frac{k^2a^2}{4}+\frac{a^2_1}{2}(\omega^2_1-\nu^2k^2_1)+\frac{a^2_2}{2}(\omega^2_2-\nu^2k^2_2)+\Delta f\left(\sum_{m\in m'}L'_m+\sum_{m\in m''}L''_m\right), \tag{42}$$

where

$$L'_m=(\beta^m_1-\beta^m_2)\left(b-\frac{a^2_1+a^2_2}{2}\right)+\frac{\omega}{2k}(\beta^m_1-\beta^m_2)\left(\frac{\omega}{k}-\beta^m_1-\beta^m_2\right)+\left(\frac{\omega}{k}-\beta^m_1\right)B^m_1-\left(\frac{\omega}{k}-\beta^i_2\right)B^m_2-\frac{1}{3}[\langle(s^m_1)^3\rangle-\langle(s^m_2)^3\rangle],$$

$$L''_m=(\beta^m_1-\beta^m_2-\beta^m_++\beta^m_-)\left(b-\frac{a^2_1+a^2_2}{2}\right)+\frac{\omega}{2k}(\beta^m_1-\beta^m_2)\left(\frac{\omega}{k}-\beta^m_1-\beta^m_2\right)+\frac{\omega}{2k}(\beta^m_+-\beta^m_-)\left(\frac{\omega}{k}-\beta^m_+-\beta^m_-\right)+\left(\frac{\omega}{k}-\beta^m_1\right)B^m_1-\left(\frac{\omega}{k}-\beta^m_2\right)B^m_2-\left(\frac{\omega}{k}-\beta^m_+\right)B^m_++\left(\frac{\omega}{k}-\beta^m_-\right)B^m_-+\frac{1}{3}[\langle(s^m_1)^3\rangle+\langle(s^m_2)^3\rangle-\langle(s^m_+)^3\rangle+\langle(s^m_-)^3\rangle],$$

and the energies $B^m_{1,2}(x),B^m_{\pm}(x)$ are associated with $u^m_{1,2},u^m_{\pm}$, respectively. Finally,

$$\langle(s^m_{1,2})^3\rangle=\frac{1}{2\pi}\int_0^{2\pi}\{2[B^m_{1,2}+(a-a_1a_2\cos\Phi)\cos\theta]\}^{3/2}d\theta,$$

$$\langle (s_{\pm}^{m})^{3} \rangle = \frac{1}{2\pi} \int_{0}^{\theta_{\pm}^{m}} \{2[B_{\pm}^{m} + (a - a_1 a_2 \cos\Phi)\cos\theta]\}^{3/2} d\theta,$$

and $\theta_{\pm}^{m} = \arccos\left[-\frac{B_{\pm}^{m}}{a - a_1 a_2 \cos\Phi}\right]$. Our averaged Lagrangian is a function of slow variables only, $\overline{L} = \overline{L}(b, a, a_{1,2}, B_{1,2}^{i}, B_{\pm}^{i}, \beta_{1,2}^{i}, \beta_{\pm}^{i}, k, k_{1,2}, \Phi)$. By taking variations of $\overline{L}$ with respect to these variables, we obtain the desired system of slow equations. The system is similar to Eqs. (16)–(32) and is presented in Appendix B. We solved these equations numerically and compared the results with the Vlasov-Ampere simulations shown in Figs. 5 and 6. As in Sec. III, for simplicity, we assumed (a) ideal phase locking ($\Phi \approx \pi/2$) between the plasma wave and the pondermotive drive, and (b) constant pump and seed amplitudes. The phase locking was indeed observed in all our simulations. The validity of assumption (b) will be discussed next.

Our system of slow variational equations includes the self-consistent evolution of both the laser pump and seed wave amplitudes. The latter are related to the plasma wave via the Manley-Rowe relations, indicating that the action fluxes $k_1 a_p^2$ and $|k_2| a_s^2$ decrease with x (the seed wave propagating in the—x direction actually increases in that direction). We found that in the kinetic regime, the depletion of the ponderomotive drive is negligible (less then 2.6% for $k_d = 1$), justifying our assumption of a fixed drive. In contrast, in the warm fluid regime ($k_d = 0.12$), the ponderomotive drive is nearly completely depleted near $x = 0$ due to the decrease of the seed wave amplitude. We illustrate this in Fig. 8. Figure 8(a) shows the amplitude of the plasma wave E_g for the constant (blue solid line) and self-consistently varying drive (red dashed line), while Fig. 8(b) shows the corresponding ponderomotive drive amplitudes. One can see that when the ponderomotive drive decreases self-consistently in the warm fluid case, the plasma wave amplitude growth is substantially reduced. Importantly, the seed wave depletion near $x = 0$ actually implies a stronger reflection of the laser wave from the plasma. This reflected (seed) wave grows from a small amplitude (due to the noise in the system, for example) near $x = 0$, to significant values at the reflecting plasma boundary. In contrast, in the strongly kinetic regime (for $k_d \gtrsim 1$, as we have found from our theory and simulations), the plasma wave grows continuously, but to much lower amplitudes, the ponderomotive drive depletion is negligible, and consequently the reflection from the plasma is weak. This effect may be important in applications, when one wishes to minimize the reflection of the pump wave.

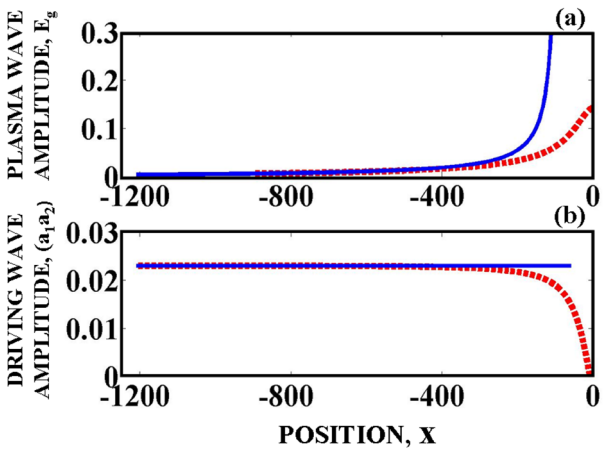

FIG. 8. The comparison between the spatial plasma wave evolution for prescribed (fixed) and self-consistent drive amplitudes in the warm fluid $k\lambda_D = 0.12$ regime. (a) Plasma wave amplitude for fixed (blue solid line) and self-consistent (red dashed line) ponderomotive drive. (b) The constant (blue solid line) and the self-consistent (red dashed line) ponderomotive driving amplitude ($a_1 a_2$ versus x, from the simulation).

V. CONCLUSIONS

In conclusion, we studied the excitation of kinetic plasma waves via stimulated Raman backscattering in a weakly nonuniform plasma. We focused on a methodical analysis of a one-dimensional plasma case where the excited plasma wave propagates in the direction of the plasma density gradient.

Numerical Vlasov-Ampere simulations show the existence of two distinct regimes of plasma wave excitation, depending on the value of $k\lambda_D$. In the warm fluid regime ($k\lambda_D \ll 1$), the main nonlinearity of the plasma wave is due to local thermal corrections in the fluid approximation, while the effect of trapped particles is negligible. In this regime, the excitation of the plasma wave discontinues prior to its reaching linear resonance (due to nonlinear dephasing). In the kinetic regime ($k\lambda_D \sim O(1)$, the dominant nonlinear effect is that of the resonant particles and the nonlocal evolution of the distribution function must be carefully analyzed. In this regime, the low density phase space regions (phase space holes) are trapped in the ponderomotive driving wave and adiabatically relocated into the bulk of the distribution, resulting in a stable, continuously autoresonant (phase locked) plasma wave over an extended plasma region.

A simplified flat-top (water bag) initial velocity distribution was assumed to allow use of the averaged Lagrangian (Whitham's) approach. The theory uses a Eulerian description for the boundaries (limiting trajectories) confining a flat-top electron distribution in phase space. The governing Lagrangian is averaged over the fast length scale associated with the driving ponderomotive potential wavelength, yielding an averaged Lagrangian for the slow variables, including the amplitudes of the driven plasma and driving laser waves. The variations with respect to these slow variables lead to a set of algebraic and ordinary differential equations that describe the autoresonant evolution of the system. The addition of the self-consistent dynamics of the pump and seed laser waves makes the theory complete and generalizes the recent results of the kinetic plasma wave excitation in an uniform plasma by a constant amplitude chirped frequency drives.[41] Generally, we found very good agreement between the predictions of the aforementioned Lagrangian theory and Vlasov simulations and many orders of amplitude improvement in the computing time in favor of the averaged Lagrangian theory for reaching sufficient accuracy.

We further generalized our theory to the case of a more realistic, Maxwellian initial velocity distribution. This case was treated within a multiple water bag model, where one

views the initial distribution as a set of superimposed thin flat-top distribution layers. We applied the Whitham's approach to this case and obtained a (more cumbersome) set of slow algebraic and ordinary differential equations similar to that found for an initially flat-top distribution. Numerical solutions of these equations were also in good agreement with the Vlasov-Ampere simulations for a Maxwellian case.

In contrast to the warm fluid regime, the plasma wave in the kinetic ($k\lambda_D \sim O(1)$) regime is excited to relatively lower amplitudes, exhibiting a continuous autoresonant evolution through an extended plasma region. Therefore, in this regime, the depletion of the pump laser wave is relatively small. Thus, the kinetic regime may be preferable in nonuniform plasma experiments for minimizing the reflection of the pump wave due to the stimulated Raman scattering.

Finally, formulation of a nonlocal, variational theory of kinetic SRS in a general adiabatic, space and time dependent plasma seems to be an interesting, but challenging goal for future studies.

ACKNOWLEDGMENTS

This work was supported by the Israel Science Foundation (Grant No. 451/10) and the US Department of Energy (Grant DE-FG02-04ER41289).

APPENDIX A: WHITHAM'S AVERAGING

This Appendix describes the averaging procedure for the case without phase space holes. The averaging in the case with phase space holes can be performed similarly. For calculating the Whitham's averaged Lagrangian, one assumes a fixed parameters case and averages over the fast phases $\theta, \theta_{1,2}$. Prior to the averaging, we use the definitions of $\Psi_{1,2}$ and $\beta_{1,2}$ (see Sec. III C) to rewrite the Lagrangian (12) as

$$L_1 = L_I + L_g + L_A, \tag{A1}$$

where

$$L_I = -\frac{1}{2}\left[\frac{1}{2\sqrt{3}}(\beta_1 - \beta_2) - \rho\right](a_1^2 + a_2^2) - \frac{1}{2\sqrt{3}}(\Psi_{1x} - \Psi_{2x})a_1 a_2 \cos\theta \cos\Phi, \tag{A2}$$

$$L_g = \left[\frac{1}{2\sqrt{3}}(\Psi_{1x} + \beta_1 - \Psi_{2x} - \beta_2) - \rho\right]U + \frac{1}{2}U_x^2 + \frac{1}{4\sqrt{3}}\left(\frac{\omega}{k} - \beta_1\right)(\Psi_{1x}^2 + \beta_1\Psi_{1x}) - \frac{1}{4\sqrt{3}}\left(\frac{\omega}{k} - \beta_2\right)(\Psi_{2x}^2 + \beta_2\Psi_{2x}) - \frac{1}{12\sqrt{3}}(\Psi_{1x}^3 + \beta_1^3 - \Psi_{2x}^3 - \beta_2^3), \tag{A3}$$

$$L_A = A_t^2 - \nu^2 A_x^2 - \rho A^2. \tag{A4}$$

We have dropped all the nonresonant terms in L_I as not contributing the dynamics. Next, we use two canonical momenta $p_{1,2} = \partial L/\partial\Psi_{1,2x}$ (conserved for fixed parameters) to express $\Psi_{1,2x}$ in terms of the total potential $(U - A^2)$

$$\Psi_{1,2x} = \frac{\omega}{k} - \beta_{1,2} - s_{1,2}, \tag{A5}$$

where, instead of $p_{1,2}$, we used $B_{1,2} = b + \frac{\omega}{2k}(\frac{\omega}{k} - \beta_{1,2}) - 2\sqrt{3}P_{1,2}$ and defined

$$s_{1,2} = \{2[B_{1,2} + (a - a_1 a_2 \cos\Phi)\cos\theta]\}^{1/2}. \tag{A6}$$

In addition to $p_{1,2}$, the "energy function"

$$F = U_x^2 + p_1\Psi_{1x} + p_2\Psi_{2x} - L_I - L_g \tag{A7}$$

is also conserved in the fixed parameters case. The reduction to the integrable, one degree of freedom problem is completed by substituting Eq. (A5) into Eq. (A7). This yields the standard "energy" conservation law for field U involving an effective potential

$$\frac{1}{2}U_x^2 + V_{eff} = F, \tag{A8}$$

where

$$V_{eff} = \frac{1}{2}\left[\frac{1}{2\sqrt{3}}(\beta_1 - \beta_2) - \rho\right](a_1^2 + a_2^2) - \frac{1}{2\sqrt{3}}a_1 a_2 \cos\Phi\cos\theta(\beta_1 - \beta_2) + \rho U - \frac{1}{2\sqrt{3}}b(\beta_1 - \beta_2) + \frac{1}{6\sqrt{3}}(s_1^3 - s_2^3) - \frac{1}{2\sqrt{3}}\left(\frac{\omega}{k} - \beta_1\right)B_1 + \frac{1}{2\sqrt{3}}\left(\frac{\omega}{k} - \beta_2\right)B_2 - \frac{1}{4\sqrt{3}}\frac{\omega}{k}(\beta_1 - \beta_2)\left(\frac{\omega}{k} - \beta_1 - \beta_2\right). \tag{A9}$$

Finally, we average in Eq. (A8) (using $\langle U_x^2\rangle = \frac{1}{2}k^2a^2$ and $U = b(x) + a(x)\cos\theta$) and substitute the result in Eq. (A7) to get the averaged Lagrangian (14) in Sec. III C.

APPENDIX B: SLOW EQUATIONS FOR A MAXWELLIAN DISTRIBUTION

This Appendix presents the system of slow equations for a Maxwellian initial distribution.

$$\sum_{m\in m'}(\beta_1^m - \beta_2^m) + \sum_{m\in m''}(\beta_1^m - \beta_2^m - \Delta u^m) = \rho/\Delta f, \tag{B1}$$

$$k^2 a/\Delta f = \sum_{m\in m'}\langle(s_1^m - s_2^m)\cos\theta\rangle + \sum_{m\in m''}\langle(2s_0^m - s_1^m - s_2^m)\cos\theta\rangle, \tag{B2}$$

$$\frac{\omega}{k} - \beta_{1,2}^m = \begin{cases} \mp\langle s_{1,2}^m\rangle & \forall m \in m', \\ \langle s_{1,2}^m\rangle & \forall m \in m'', \end{cases} \tag{B3}$$

$$\Delta u^m/2 = \langle s_0^m\rangle \quad \forall m \in m'', \tag{B4}$$

$$a_{1,2}(\rho - \omega_{1,2}^2 + \nu^2 k_{1,2}^2) = \frac{k^2}{2} a_{2,1} a \cos\Phi, \tag{B5}$$

$$B_{1,2}^m - b + \frac{\omega}{k}\left(\beta_{1,2}^m - \frac{\omega}{2k}\right) + \frac{a_1^2 + a_2^2}{2} = C_{1,2}^m, \quad \forall m \in m', m'' \tag{B6}$$

$$\left\{ ka^2 - \frac{\omega \Delta f}{k^2} \sum_{m \in m', m''} \left[B_1^m - B_2^m + \frac{1}{2}(\beta_1^m - \beta_2^m)\left(\frac{2\omega}{k} - \beta_1^m - \beta_2^m\right)\right]\right\}_x = k^2 a_1 a_2 a \sin\Phi, \tag{B7}$$

$$\begin{gathered}(k_1 a_1^2)_x = -(k_2 a_2^2)_x = \frac{k^2}{2\nu^2} a_1 a_2 a \sin\Phi, \\ \Phi_x = k_1 - k_2 - k.\end{gathered} \tag{B8}$$

Here, we set $B_+^m = B_-^m \equiv B_0^m$ and, consequently, $\langle s_+^m \rangle = \langle s_-^m \rangle \equiv \langle s_0^m \rangle$ for the mth layer. We also defined $\Delta u^m \equiv \beta_+^m - \beta_-^m = 2\left[\frac{\omega}{k^*} - \beta_1^{m*}\right]$ (k^* and β_1^{m*} being the values of k, β_1^m at $x = x^{m*}$, where the hole is formed in the mth layer).

[1]W. L. Kruer, *The Physics of Laser-Plasma Interaction* (Addison-Wesley, New-York, 1988).
[2]J. Lindl, *Inertial Confinement Fusion. The Quest for Ignition and Energy Gain Using Indirect Drive* (Springer, New York, 1998).
[3]J. Lindl, Phys. Plasma **2**, 3933 (1995).
[4]J. F. Drake, P. K. Kaw, Y. C. Yee, G. Schmidt, C. S. Liu, and M. N. Rosenbluth, Phys. Fluids **17**, 778 (1974).
[5]D. W. Forslund, J. M. Kindel, and E. L. Lindman, Phys. Fluids **18**, 1002 (1975).
[6]D. W. Phillion, D. L. Banner, E. M. Campbell, R. E. Turner, and K. G. Estabrook, Phys. Fluids **25**, 1434 (1982).
[7]J. C. Fernandez, J. A. Cobble, D. S. Montomery, M. D. Wilke, and B. B. Afeyan, Phys. Plasmas **7**, 3743 (2000).
[8]H. X. Vu, D. F. DuBois, and B. Bezzerides, Phys. Plasmas **9**, 1745 (2002).
[9]G. Shvets, N. J. Fisch, A. Pukhov, and J. Meyer-ter-Vehn, Phys. Rev. Lett. **81**, 4879 (1998).
[10]V. M. Malkin, G. Shvets, and N. J. Fisch, Phys. Rev. Lett. **82**, 4448 (1999).
[11]V. M. Malkin, G. Shvets, and N. J. Fisch, Phys. Plasmas **7**, 2232 (2000).
[12]N. A. Yampolsky, N. J. Fisch, V. M. Malkin, E. J. Valeo, R. Lindberg, J. Wurtele, J. Ren, S. Li, A. Morozov, and S. Suckewer, Phys. Plasmas **15**, 113104 (2008).
[13]P. Bertrand, G. Baumann, and M. R. Feix, Phys. Lett. A **29**, 489 (1969).
[14]P. Bertrand and M. R. Feix, Phys. Lett. A **28**, 68 (1968).
[15]D. A. Tidman and H. M. Stainer, Phys. Fluids **8**, 345 (1965).
[16]R. L. Dewar and J. Lindl, Phys. Fluids **15**, 820 (1972).
[17]T. Kakutani and N. Sugimoto, Phys. Fluids **17**, 1617 (1974).
[18]T. P. Coffey, Phys. Fluids **14**, 1402 (1971).
[19]J. L. Kline, D. S. Montgomery, B. Bezzerides, J. A. Cobble, D. F. Dubbois, R. P. Jhonson, H. A. Rose, L. Yin, and H. X. Vu, Phys. Rev. Lett. **94**, 175003 (2005).
[20]J. L. Kline, D. S. Montgomery, L. Yin, D. F. Dubois, B. J. Albright, B. Bezzerides, J. A. Cobble, E. S. Dodd, D. F. Dubois, J. C. Fernandez, R. P. Johnson, J. M. Kindel, and H. A. Rose, Phys. Plasmas **13**, 055906 (2006).
[21]B. J. Winjum, J. Fahlen, and W. B. Mori, Phys. Plasmas **14**, 102104 (2007).
[22]R. R. Lindberg, A. E. Charman, and J. S. Wurtele, Phys. Plasmas **14**, 122103 (2007).
[23]D. E. Hinkel, M. D. Rosen, E. A. Williams, A. B. Langdon, C. H. Still, D. A. Callahan, J. D. Moody, P. A. Michel, R. P. J. Town, R. A. London, and S. H. Langer, Phys. Plasmas **18**, 056312 (2011).
[24]R. K. Kirkwood, P. Michel, R. London, J. D. Moody, E. Dewald, L. Yin, J. Kline, D. Hinkel, D. Callahan, N. Meezan, E. Williams, L. Divol, B. L. Albright, K. J. Bowers, E. Bond, H. Rose, Y. Ping, T. L. Wang, C. Joshi, W. Seka, N. J. Fisch, D. Turnbull, S. Suckewer, J. S. Wurtele, S. Glenzer, L. Suter, C. Haynam, O. Landen, and B. J. Macgowan, Phys. Plasmas **18**, 056311 (2011).
[25]J. D. Moody, P. Michel, L. Divol, R. L. Berger, E. Bond, D. K. Bradley, D. A. Callahan, E. L. Dewald, S. Dixit, M. J. Edwards, S. Glenn, A. Hamza, C. Haynam, D. E. Hinkel, N. Izumi, O. Jones, J. D. Kilkenny, R. K. Kirkwood, J. L. Kline, W. L. Kruer, G. A. Kyrala, O. L. Landen, S. LePape, J. D. Lindl, B. J. MacGowan, N. B. Meezan, A. Nikroo, M. D. Rosen, M. B. Schneider, D. J. Strozzi, L. J. Suter, C. A. Thomas, R. P. J. Town, K. Widmann, E. A. Williams, L. J. Atherton, S. H. Glenzer, and E. I. Moses, Nature Phys. **8**, 344 (2012).
[26]R. R. Lindberg, A. E. Charman, and J. S. Wurtele, Phys. Plasmas **15**, 055911 (2008).
[27]D. Benisti and L. Gremillet, Phys. Plasmas **14**, 042304 (2007).
[28]M. S. Hur, S. H. Yoo, and H. Suk, Phys. Plasmas **14**, 033104 (2007).
[29]T. L. Wang, D. Michta, R. R. Lindberg, A. E. Charman, S. F. Martins, and J. S. Wurtele, Phys. Plasmas **16**, 123110 (2009).
[30]D. Benisti, N. A. Yampolsky, and N. J. Fisch, Phys. Plasmas **19**, 013110 (2012).
[31]C. S. Liu, M. N. Rosenbluth, and R. B. White, Phys. Fluids **17**, 1211 (1974).
[32]O. Yaakobi, L. Friedland, R. R. Lindberg, A. E. Charman, and G. Penn, Phys. Plasmas **15**, 032105 (2008).
[33]V. I. Veksler, J. Phys. (USSR) **9**, 153 (1945).
[34]E. M. McMillan, Phys. Rev. **68**, 143 (1945).
[35]J. Fajans and L. Friedland, Am. J. Phys. **69**, 1096 (2001).
[36]L. Friedland, Scolarpedia **4**, 5473 (2009).
[37]L. Friedland, Phys. Rev. Lett. **69**, 1749 (1992).
[38]G. B. Whitham, *Linear and Nonlinear Waves* (Wiley, New York, 1974).
[39]L. Friedland, Phys. Rev. E **55**, 1929 (1997).
[40]L. Friedland, Phys. Plasmas **5**, 645 (1998).
[41]P. Khain and L. Friedland, Phys. Plasmas **17**, 102308 (2010).
[42]O. Polomarov and G. Shvets, Phys. Plasmas **13**, 054502 (2006).
[43]We note that in Ref. 32 at one point the text mistakenly refers to wave propagating in the negative x-direction as moving to higher plasma density.
[44]G. J. Morales and T. M. O'Neil, Phys. Rev. Lett. **28**, 417 (1972).
[45]R. L. Dewar, Phys. Fluids **15**, 712 (1972).
[46]T. Chapman, S. Huller, P. E. Masson-Laborde, W. Rozmus, and D. Pesme, Phys. Plasmas **17**, 122317 (2010).
[47]T. Chapman, S. Huller, P. E. Masson-Laborde, A. Heron, D. Pesme, and W. Rozmus, Phys. Rev. Lett. **108**, 145003 (2012).
[48]E. A. Williams, B. I. Cohen, L. Divol, M. R. Dorr, J. A. Hittinger, D. E. Hinkel, A. B. Langdon, R. K. Kirkwood, D. H. Froula, and S. H. Glenzer, Phys. Plasmas **11**, 231 (2004).
[49]L. Friedland, P. Khain, and A. Shagalov, Phys. Rev. Lett. **96**, 225001 (2006).
[50]L. Friedland and P. Khain, Phys. Plasmas **14**, 082110 (2007).
[51]I. B. Bernstein, J. M. Greene, and M. D. Kruskal, Phys. Rev. **108**, 546 (1957).
[52]H. L. Berk, B. N. Breizman, J. Candy, M. Pekker, and N. V. Petviashvilli, Phys. Plasmas **6**, 3102 (1999).
[53]D. Yu. Eremin and H. L. Berk, Phys. Plasmas **9**, 772 (2001).
[54]D. Yu. Eremin and H. L. Berk, Phys. Plasmas **11**, 3621 (2004).
[55]I. Y. Dodin and N. J. Fisch, Phys. Plasmas **19**, 012103 (2012).